# Investigation of a Novel Interleaved Buck Converter for Renewable Energy Applications: Design and Analysis

Madhuchandra Popuri[1], Veera Venkata Subrahmanya Kumar Bhajana[2*], Manoj Kumar Maharana[1]

[1] School of Electrical Engineering, KIIT University, Campus-3, 751024 Bhubaneswar, Odisha, India
[2] School of Electronics Engineering, KIIT University, Campus-12, 751024 Bhubaneswar, Odisha, India
* Corresponding author, e-mail: bvvs.kumarfet@kiit.ac.in

**Abstract**

In this paper, a new interleaved buck converter with soft-switching is investigated. The soft-switching condition, zero voltage zero current switching (ZVZCS) of IGBTs during turn-on is obtained with the help of a soft-switching cell that includes active and passive devices that is incorporated in the interleaved buck converter (IBC). The presence of the soft-switching cell reduces the switching losses and improves the overall efficiency. The IGBTs in the converter achieved ZVZCS turn on operations, while converter is operated under both light and heavy loads. The principles of operation and theoretical aspects of the proposed converter system 400 V / 110 V / 2.5 kW are verified with simulation analysis.

**Keywords**

interleaved buck converter, zero voltage switching (ZVS), zero current switching (ZCS), zero voltage zero current switching (ZVZCS)

## 1 Introduction

In recent days, step-down, cost effective and efficient converters operating at high power levels are widely used in renewable energy applications. High voltage-gain ratio and decreased voltage stresses of power switches are achieved through a non-isolated interleaved soft-switching bidirectional dc–dc converter (BDC) with a T-type neutral point-clamped circuit (NPCC) based built-in transformer (BT) [1] as unlike conventional interleaved buck–boost BDC [2]. Similarly, another literature focusing on BDC with in-built transformer [3] was implemented that achieves a very high step-down conversion ratio. Nevertheless, it works well only with low voltage and low power applications, and also it has increased number of devices.

A very high switching frequency and low output power zero voltage transition (ZVT) interleaved buck converter (IBC) with GaN devices and a variable coupled inductor (VCI) [4] and an inverse coupled inductor (ICI) based BDC [5] aims at reducing circulating energy and also minimizes the resonant transition period. By altering the values of coupling coefficient of VCI, the converter is allowed to operate for an extended range of input and output voltages while improving the zero voltage transition range. However, inverse coupled inductor (ICI) though giving considerable output power, is suitable only for

limited range of operating voltages. Another synchronous rectifier buck converter (SRBC) [6] is also realized with GaN switching devices, which is controlled with error free phase control method that avoids the usage of zero-crossing detection (ZCD). This topology is used in applications for obtaining high voltage and high power.

To limit the duty cycles and to achieve better efficiency, a dual coupled inductor (DCI) based synchronous buck converter (SBC) [7] and Multiphase asymmetric buck converter (MABC) [8] without auxiliary circuit have been implemented. The ZVS condition is achieved with the help of a series capacitor and leakage inductance. However, this is suitable for very low power and low voltage applications in spite of operating at a high switching frequency. An active clamp based non-isolated interleaved buck/boost bidirectional converter (IBB-BDC) [9] is developed with the ZVS operation. The soft-switching is obtained for boost and as well as buck modes irrespective of duty cycle or load condition. Apart from the non-isolated IBCs, researchers focused on isolated interleaved fly-back converters (IIFBC) [10] with active clamp circuit (ACC) that reduce voltage stresses. Though ZVS condition is achieved, the device count is increased and the circulating energy is also reduced.

To minimize the current ripple, voltage stresses and device count, this research is focused to develop an efficient soft-switched interleaved buck converter. This paper introduces a novel interleaved buck converter with ZVZCS condition, which has an additional auxiliary cell with a few active and passive components. The minimized switching losses, improved efficiency and soft-switching are the main merits of this proposed converter without considerably increasing auxiliary cell losses. To validate the soft-switching characteristics, the presented converter design with 400 V / 110 V / 2.5 kW is verified by its simulation. Section 2 describes the proposed circuit and its operating principles and Section 3 presents simulation results.

## 2 Description and operating principles of the proposed converter

The circuit diagram of the proposed ZVZCS converter is shown in Fig. 1. The converter consists of two main switches $S_1$, $S_2$. Each of these switches is provided with an inductor and a capacitor, namely, $L_a$, $C_a$, $L_b$ and $C_b$. $L_a$ and $C_a$ along with the diode, $D_a$ acts as an auxiliary cell. Similarly, $L_b$ and $C_b$ along with the diode, $D_b$ acts as another auxiliary cell. These are shown in Fig. 1. The proposed converter operation is described with the aid of voltage and current waveforms of $L_1$, $L_2$, $S_1$, $S_2$, $L_a$, $L_b$, $C_a$ and $C_b$ shown in Fig. 2. The buck mode operation is divided into three states and six intervals.

### 2.1 State 1 ($t_0$-$t_1$ and $t_1$-$t_2$)

During this mode, switch, $S_1$ is turned-on at time $t_0$. The current in the auxiliary inductor, $L_a$ increases. The capacitor, $C_a$ starts charging. Since the voltage across $S_1$ and the current through it are zero, ZVZCS is achieved for $S_1$. The voltage across the capacitor, $C_a$ reaches to the value of input voltage, $V_{in}$ at $t_1$. At $t_1$, the voltage across $C_a$ and
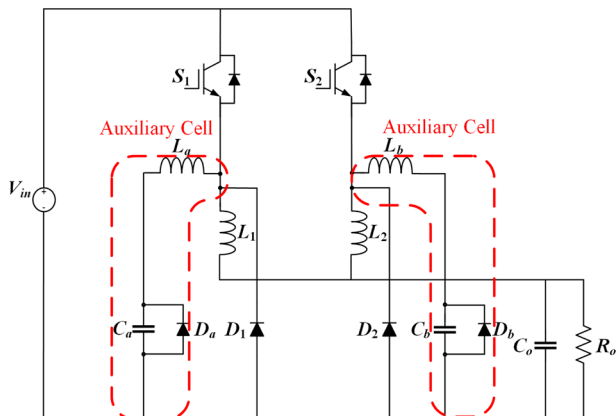
**Fig. 1** Proposed soft-switching interleaved buck converter
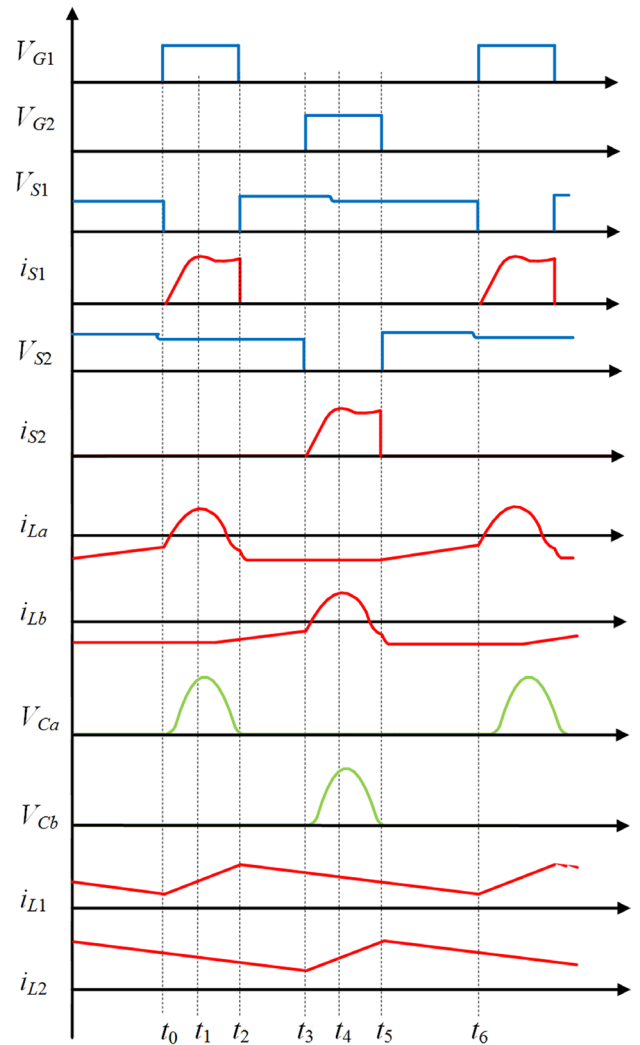
**Fig. 2** Key waveforms of the proposed converter

current through $L_a$ both starts decreasing and reaches to zero at $t_2$. The current, $i_{L1}$ increases linearly and the current, $i_{L2}$ decreases linearly. Throughout this interval, $L_a$ and $C_a$ both resonate with each other and hence this mode is considered as resonant mode. The equivalent schematics with current flow are shown in Fig. 3(a) and (b).

The current and voltage equations are expressed as follows:

$$-V_{in} + V_{La} + V_{Ca} = 0, \tag{1}$$

$$V_{La} = V_{in} - V_{Ca}, \tag{2}$$

$$i_{La}(t) = i_{La}(t_0)\cos\omega_a(t - t_0), \tag{3}$$

$$V_{Ca}(t) = Z_a\sin\omega_a(t - t_0), \tag{4}$$

where $Z_a = \sqrt{\dfrac{L_a}{C_a}}$; $\omega_a = \dfrac{1}{\sqrt{L_a C_a}}$.
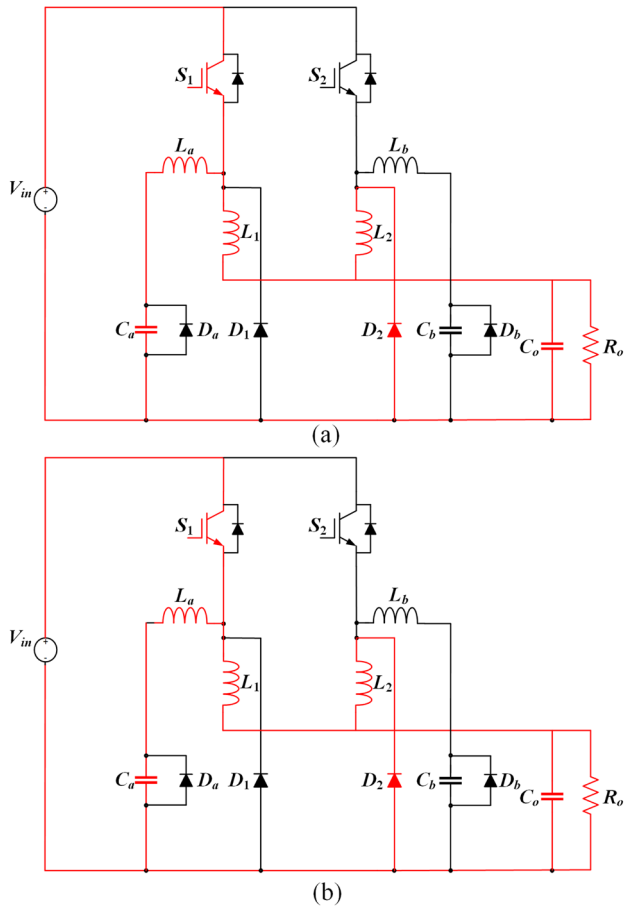
**Fig. 3** Equivalent circuits of state 1; (a) $t_0$–$t_1$ and (b) $t_1$–$t_2$



**Fig. 4** Equivalent circuits of state 2 time intervals; (a) $t_2$–$t_3$ and (b) $t_5$–$t_6$

$$-V_{in} + V_{L1} + V_{Co} = 0 \tag{5}$$

$$V_{L1} = V_{in} - V_o \tag{6}$$

$$L_1 \frac{di_{L1}}{dx} = V_{in} - V_o \tag{7}$$

$$i_{L1}(t) = \frac{V_{in} - V_o}{L_1}(t - t_0) + i_{L1}(t_0) \tag{8}$$

$$i_{L2}(t) = -\frac{V_o}{L_2}(t - t_0) + i_{L2}(t_0) \tag{9}$$

## 2.2 State 2 ($t_2$-$t_3$ and $t_5$-$t_6$)

At time $t_2$, switch, $S_2$ is turned off and the inductors, $L_1$ and $L_2$ both conduct the current through the load. The currents, $i_{L1}$ and $i_{L2}$ both decrease linearly, till $t_3$. Similarly, the same operation occurs during the interval, $t_5$-$t_6$. At $t_5$, switch $S_1$ is turned off and the inductors, $L_1$ and $L_2$ both conduct current through the load. The equivalent schematics with current flow are shown in Fig. 4(a) and (b).

$$i_{L1}(t) = -\frac{V_o}{L_1}(t - t_2) + i_{L1}(t_2) \tag{10}$$

$$i_{L2}(t) = -\frac{V_o}{L_2}(t - t_2) + i_{L2}(t_2) \tag{11}$$

## 2.3 State 3 ($t_3$-$t_4$ and $t_4$-$t_5$)

During this state, switch, $S_2$ is turned-on at time $t_4$. The current in the auxiliary inductor, $L_b$ increases. The capacitor, $C_b$ starts charging. At $t_4$, the voltage across $C_b$ reaches to the input voltage, $V_{in}$. The current through $L_b$ and voltage across $C_b$ both starts decreasing and will become zero at time, $t_5$. Throughout this interval, the current, $i_{L2}$ increases linearly and the current, $i_{L1}$ decreases linearly. Since the voltage across $S_2$ and the current through it are zero, ZVZCS is achieved for $S_2$.

Throughout this interval, $L_b$ and $C_b$ both resonate with each other and hence this mode is also considered as resonant mode. The equivalent schematics with current flow are shown in Fig. 5(a) and (b). The current and voltage equations are expressed as follows:
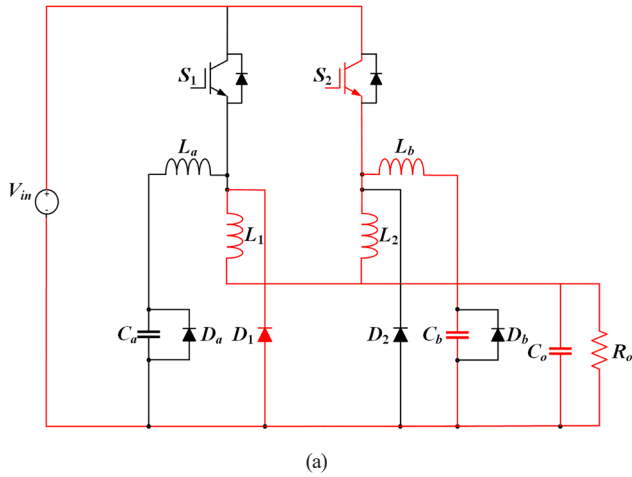
(a)
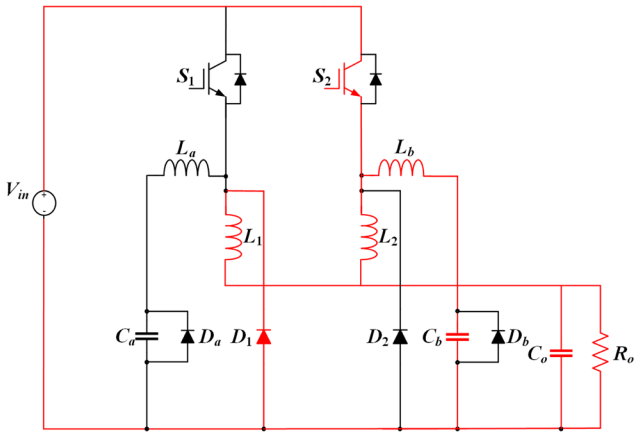


(b)

**Fig. 5** Equivalent circuits of state 3 interval; (a) $t_3-t_4$ and (b) $t_4-t_5$

$$-V_{in} + V_{Lb} + V_{Cb} = 0, \tag{12}$$

$$i_{Lb}(t) = i_{Lb}(t_3)\cos\omega_b(t-t_3),$$

where $Z_b = \sqrt{\dfrac{L_b}{C_b}}$; $\omega_b = \dfrac{1}{\sqrt{L_b C_b}}$. \hfill (13)

**Table 1** Design parameters

| Parameter | Symbol | Value |
|---|---|---|
| Input voltage | $V_{in}$ | 400 V |
| Output power | $P_o$ | 2.5 kW |
| Switching frequency | $f_{sw}$ | 50 kHz |
| Resonant inductors | $L_a, L_b$ | 45 µH |
| Resonant capacitors | $C_a, C_b$ | 20 nF |
| Inductors | $L_1, L_2$ | 200 µH |
| Output capacitor | $C_o$ | 470 µF |

$$V_{Cb}(t) = Z_b \sin\omega_b(t-t_3) \tag{14}$$

$$V_{L2} = V_{in} - V_o \tag{15}$$

$$i_{L2}(t) = \frac{V_{in} - V_o}{L_2}(t-t_3) + i_{L2}(t_3) \tag{16}$$

$$V_{L1} = V_{Co} \tag{17}$$

$$i_{L1}(t) = -\frac{V_o}{L_1}(t-t_3) + i_{L1}(t_3) \tag{18}$$

## 3 Simulation analysis

The design simulations of the proposed converter are carried out using MATLAB Simulink. The design parameters considered are mentioned in Table 1. Firstly, the simulations are performed when the converter is operated at 2.5 kW with the voltage 400 V as input voltage and obtained 110 V as output voltage.

Fig. 6 shows the voltage and current waveforms of $S_1$ and $S_2$. It is observed that the turn on transition of IGBTs achieved ZVZCS condition without any voltage and current stresses. However, the turn off transition of IGBTs is hard switched. Fig. 7 shows voltage and current waveforms of $L_1$, $L_2$, $D_1$ and $D_2$. It can be seen from Fig. 7, the peak currents
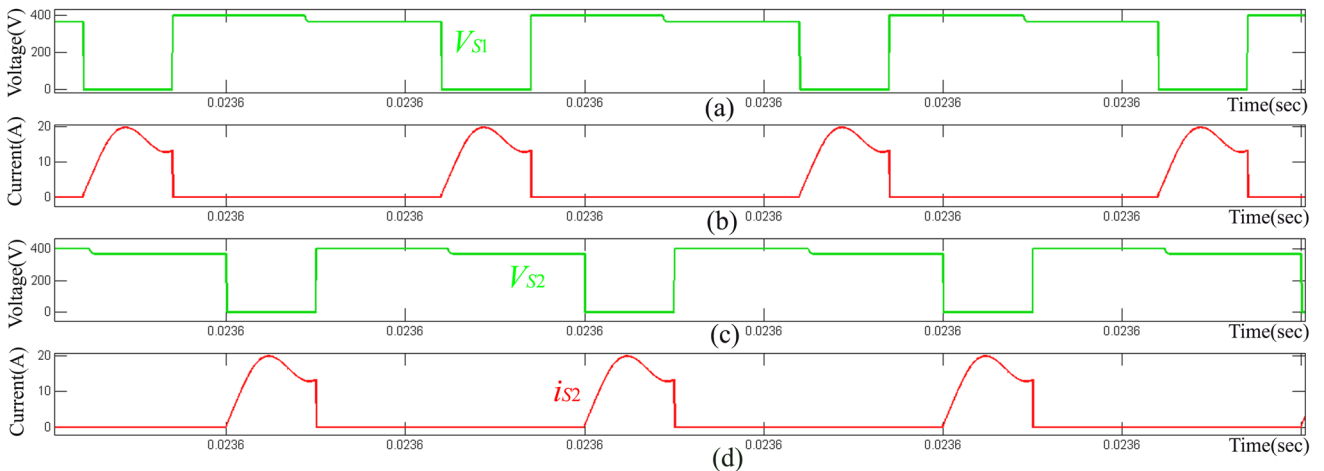


**Fig. 6** Simulated waveforms; (a) Collector to emitter voltage of $S_1$: $V_{S1}$; (b) Collector current of $S_1$: $i_{S1}$; (c) Collector to emitter voltage of $S_2$: $V_{S2}$; (d) Collector current of $S_2$: $i_{S2}$

through $L_1$, $L_2$ reach to the input current level, 22 A. The voltages across $D_1$, $D_2$ reach to input voltage level, 400 V.

Fig. 8 shows the current through resonant inductors, $i_{La}$, $i_{Lb}$ and voltages across resonant capacitors, $V_{ca}$, $V_{cb}$. The peak currents through $L_a$, $L_b$, are less than the maximum input current and the resonant capacitors $C_a$, $C_b$ charge and discharge during the resonating periods, $t_0$-$t_2$ and $t_3$–$t_5$ as shown in Fig. 2. Similarly, voltages across and currents through $D_a$, $D_b$ are depicted in Fig. 9. It can be seen that the diodes $D_a$, $D_b$ turn on and turn off with ZVS condition. However, there is some current stress present in $D_a$, $D_b$ during turn on, which is 15 A.

The capability of soft switching turn on conditions of IGBTs, $S_1$, $S_2$ are verified under light and heavy load conditions. The light load condition is considered when the converter output voltage is 200 V and output current is 6.5 A. The overlapping period between current and voltage waveforms is very short and has negligible turn on losses and hence the turn on of the switches can be considered as soft switched. The heavy load condition is considered at 2.5 kW output power which is observed that the overlapping period slightly increases than that of light load condition. Fig. 10 shows $V_{S1}$ and $i_{S1}$ during turn on and turn off at light and heavy load conditions.

Fig. 11 shows turn on and turn off transitions, when the converter is operating without and with auxiliary cells at heavy load condition It is observed that the overlapping
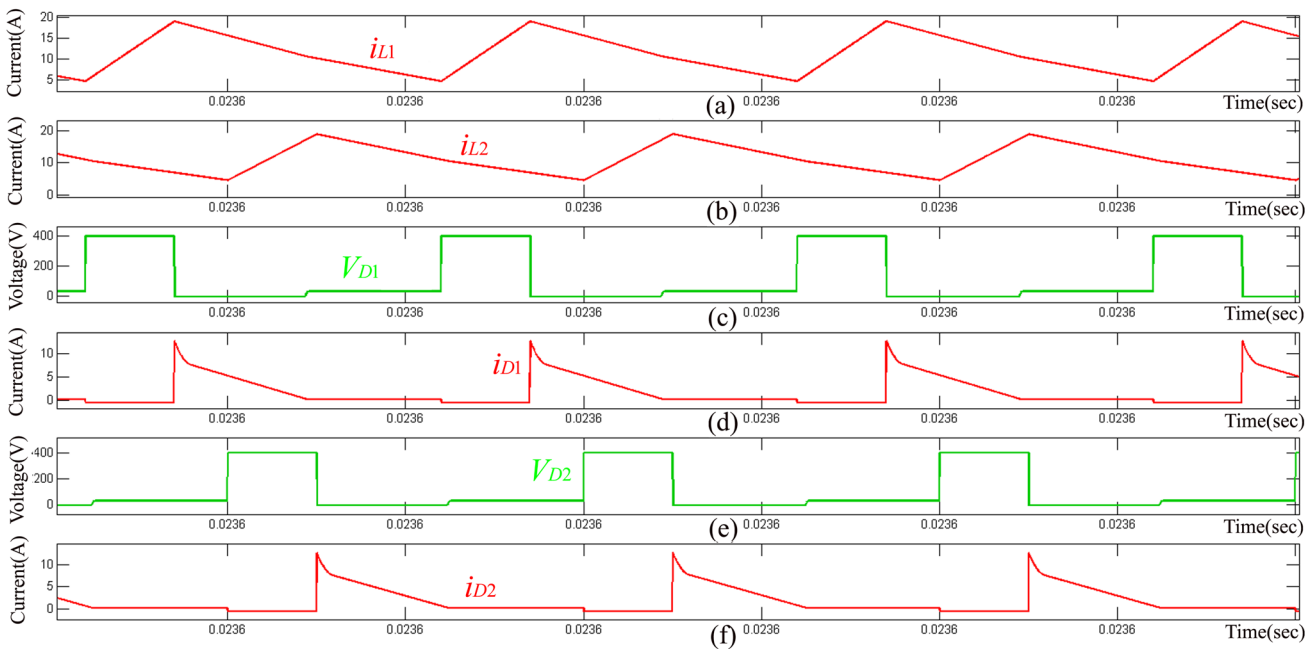


**Fig. 7** Simulated waveforms; (a) Current through inductor, $L_1$: $i_{L1}$; (b) Current through inductor, $L_2$: $i_{L2}$; (c) Voltage across diode, $D_1$: $V_{D1}$; (d) Current through diode, $D_1$: $i_{D1}$; (e) Voltage across diode, $D_2$: $V_{D2}$; (f) Current through diode, $D_2$: $i_{D2}$
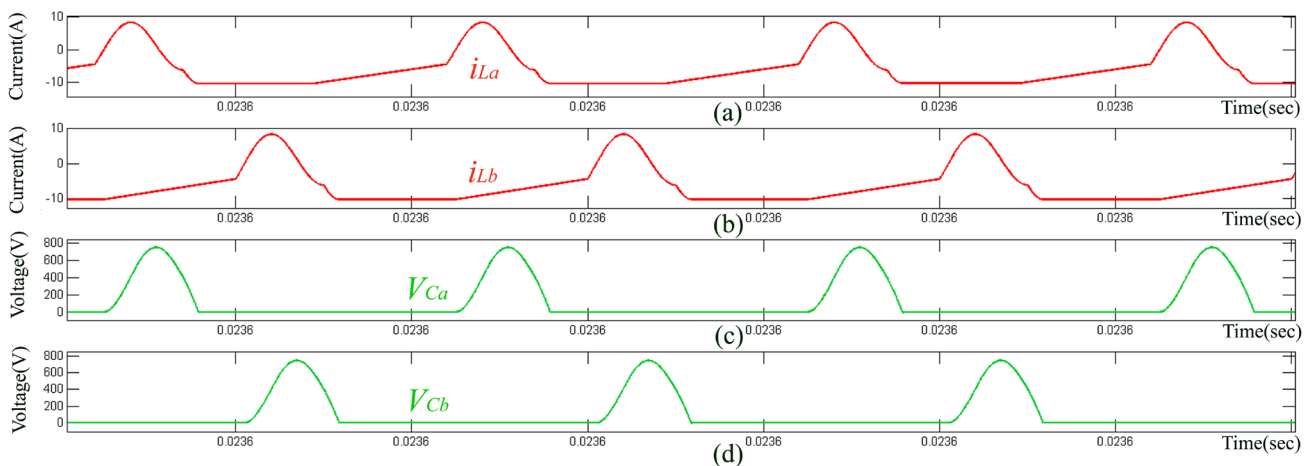


**Fig. 8** Simulated waveforms; (a) Current through resonant inductor, $L_a$: $i_{La}$; (b) Current through resonant inductor, $L_b$: $i_{Lb}$; (c) Voltage across resonant capacitor, $C_a$: $V_{Ca}$; (d) Voltage across resonant capacitor, $C_b$: $V_{Cb}$
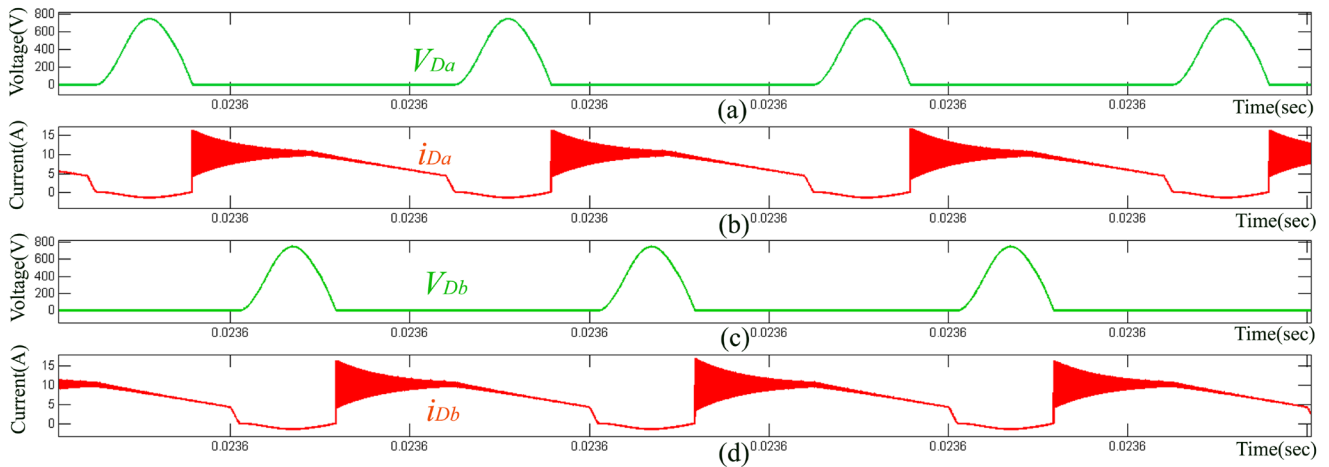
**Fig. 9** Simulated waveforms; (a) Voltage across diode, $D_a$: $V_{Da}$; (b) Current through diode, $D_a$: $i_{Da}$; (c) Voltage across diode, $D_b$: $V_{Db}$; (d) Current through diode, $D_b$: $i_{Db}$
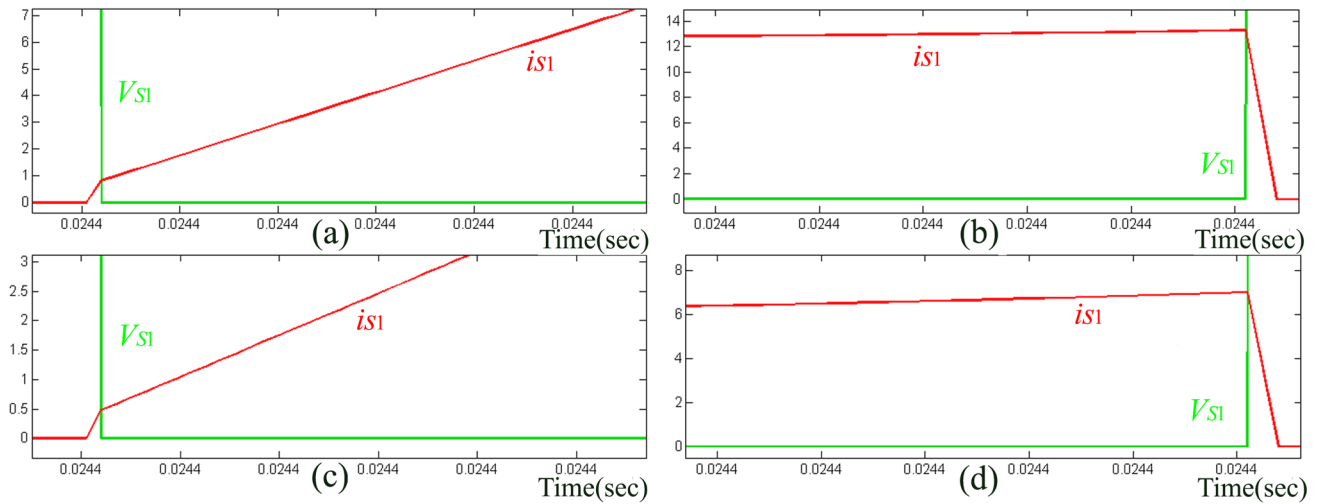


**Fig. 10** Waveforms of $S_1$: $V_{S1}$, $i_{S1}$; (a) Turn on transition under heavy load condition; (b) Turn off transition under heavy load condition; (c) Turn on transition under light load condition; (d) Turn off transition under light load condition
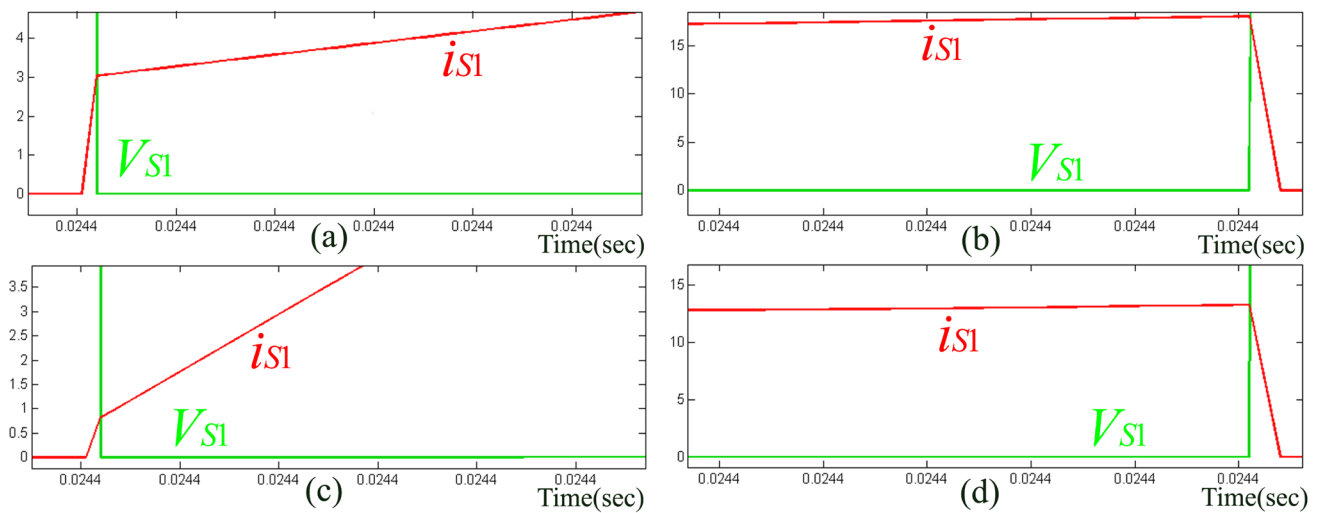


**Fig. 11** Waveforms of $S_1$: $V_{S1}$, $i_{S1}$; (a) Turn on transition without auxiliary cell; (b) Turn off transition without auxiliary cell; (c) Turn on transition with auxiliary cell; (d) Turn off transition with auxiliary cell

period between the voltage, $V_{S1}$ and current, $i_{S1}$ has been increased during turn on and turn off condition of $S_1$.

## 4 Conclusion

In this paper, the design analysis of a new interleaved buck converter is presented. The proposed converter is operated at 400 V / 110 V / 2.5 kW with the switching frequency being 50 kHz. The operating principles and its simulation

analysis are also discussed. The topology of IBC is derived from the conventional interleaved buck converter with two simple auxiliary cells. The soft switching of this topology can withstand for light and heavy loads without increasing additional losses. The proposed topology is the alternate solution for the industry with better efficiency especially for high power applications.

## References

[1] Yan, Z., Zeng, J., Lin, W., Liu, J. "A Novel Interleaved Nonisolated Bidirectional DC–DC Converter With High Voltage-Gain and Full-Range ZVS", IEEE Transactions on Power Electronics, 35(7), pp. 7191–7203, 2020.
https://doi.org/10.1109/TPEL.2019.2957451

[2] Waffler, S., Biela, J., Kolar, J. W. "Output ripple reduction of an automotive multi-phase bi-directional dc-dc converter", In: 2009 IEEE Energy Conversion Congress and Exposition, San Jose, CA, USA, 2009, pp. 2184–2190.
https://doi.org/10.1109/ECCE.2009.5316346

[3] Zheng, Y., Li, S., Smedley, K. M. "Nonisolated High Step-Down Converter With ZVS and Low Current Ripples", IEEE Transactions on Industrial Electronics, 66(2), pp. 1068–1079, 2019.
https://doi.org/10.1109/TIE.2018.2833047

[4] Pajnić, M., Pejović, P. "Zero-Voltage Switching Control of an Interleaved Bi-Directional Buck–Boost Converter With Variable Coupled Inductor", IEEE Transactions on Power Electronics, 34(10), pp. 9562–9572, 2019.
https://doi.org/10.1109/TPEL.2019.2893703

[5] Huang, X., Lee, F. C., Li, Q., Du, W. "High-Frequency High-Efficiency GaN-Based Interleaved CRM Bidirectional Buck/Boost Converter with Inverse Coupled Inductor", IEEE Transactions on Power Electronics, 31(6), pp. 4343–4352, 2016.
https://doi.org/10.1109/TPEL.2015.2476482

[6] Liu, Y. C., Syu, Y. L., Dung, N. A., Chen, C., Chen, K. D., Kim, K. A. "High-Switching-Frequency TCM Digital Control for Bidirectional-Interleaved Buck Converters Without Phase Error for Battery Charging", IEEE Journal of Emerging and Selected Topics in Power Electronics, 8(3), pp. 2111–2123, 2020.
https://doi.org/10.1109/JESTPE.2019.2954602

[7] Marvi, F., Adib, E., Farzanehfard, H. "Efficient ZVS Synchronous Buck Converter with Extended Duty Cycle and Low-Current Ripple", IEEE Transactions on Industrial Electronics, 63(9), pp. 5403–5409, 2016.
https://doi.org/10.1109/TIE.2016.2558483

[8] Hajiheidari, M., Farzanehfard, H., Esteki, M. "Asymmetric ZVS Buck Converters With High-Step-Down Conversion Ratio", IEEE Transactions on Industrial Electronics, 68(9), pp. 7957–7964, 2021.
https://doi.org/10.1109/TIE.2020.3013538

[9] Mohammadi, M. R. "An Active-Clamping ZVS Interleaved Buck/ Boost Bidirectional Converter With One Auxiliary Switch", IEEE Transactions on Industrial Electronics, 67(9), pp. 7430–7438, 2020.
https://doi.org/10.1109/TIE.2019.2945284

[10] Cheng, H. L., Chang, Y. N., Yen, H. C., Hua, C. C., Su, P. S. "An Interleaved Flyback-Typed LED Driver With ZVS and Energy Recovery of Leakage Inductance", IEEE Transactions on Power Electronics, 34(5), pp. 4497–4508, 2019.
https://doi.org/10.1109/TPEL.2018.2864223